Reviews of Electromagnetics, Vol. V, 2026
EuCAP 2026 Special Issue
DOI: 10.53792/RoE/2026/26002

Reviews of Electromagnetics
EuCAP 2026 Special Issue

A Deployable S-Band Yagi-Uda Antenna for a 3U CubeSat Based on a Pantograph Mechanism

Conor M. Lambe[1]*, Geoffrey S. Hilton[1], Andrew C. M. Austin[1]

Abstract
An eight element Yagi-Uda antenna utilising a deployable pantograph mechanism operating across the 2.4 GHz ISM band is proposed. The mechanism permits the antenna structure to stow into a compact volume prior to deployment, with a stowed volume of 29.7 cm^3 and deployed-to-stowed length ratio of 6.7. The antenna and pantograph mechanism fits on the 'small' face of a 3U CubeSat ($30 \times 10 \times 10$ cm). In the fully deployed state the antenna presents a gain of 11.9 dBi at the operational frequency of 2.45 GHz, with an $|S_{11}|$ of -17.2 dB. The side lobe levels are measured to be -9.3 and -15 dB in the E and H plane respectively, and the corresponding beamwidths are 52.3° and 42.0°. A fractional bandwidth of 22.9% is found, and the measured results show a good agreement to the simulated results. The fabricated antenna performance is evaluated on a model of 3U CubeSat chassis, and additional measurements are taken in the case of a deployment failure. It is found that the antenna functions with slightly reduced performance in the case of a partial deployment failure, with a gain of 11.1 dBi, and moderately reduced performance in the case of a full failure, with a gain of 9.3 dBi.

Key terms
Antenna; CubeSat; Yagi-Uda; UHF; Deployable; Small-Satellite

[1] *Communication Systems and Networks Group, School of Electrical, Electronic, and Mechanical Engineering, University of Bristol, Bristol, United Kingdom*
***Corresponding author**: cm.lambe@bristol.ac.uk

Received: 25/05/2026, Accepted: 28/10/2026, Published: xx/11/2026

1. Introduction

In recent decades there has been a significant increase in the number of small satellites launched, owing to increased technical capabilities and reduced development and launch costs [1]. The European Space Agency's 2024 Report on the Space Economy found that of the 2,940 satellites launched in 2023, approximately 13% had a launch mass below 15 kg. If Starlink satellites are omitted from this data, it can be seen that ∼41% of these remaining launches consisted of sub-15 kg satellites [2]. Satellites following the CubeSat standard [3] make up a large fraction of these launches, with 67.8% being in the 1, 3, or 6U form factors ($10/30/60 \times 10 \times 10$ cm) [4]. CubeSats have been used for many applications previously restricted to larger satellites, such as earth observation and satellite communications [5].

The limited size of CubeSat platforms presents a challenge in the design of the systems and components. In particular, the implementation of high-gain antennas is complicated due to the relatively large physical apertures required. While CubeSat antennas operating at X-Band and Ka-Band have achieved high gain [6, 7], it remains challenging to design high gain antennas at lower frequencies, e.g., UHF, L-, and S-band platforms, as the longer wavelengths require physically large apertures [8, 9]. This issue remains significant, as these lower frequencies have been widely allocated internationally for both satellite communications and ISM applications (such as IoT device communication and sensing). In the case of satellite communications, a reduced gain impacts the signal-to-noise ratio of the communications link, resulting in lower-order modulation schemes and reduced data rates. Since IoT devices typically use low-gain antennas due to size constraints, the link budget must be closed on the receiving side of the link by using a high-gain antenna. To address these challenges, deployable antennas are commonly used on satellites to maximise the available aperture once in orbit, whilst minimising the stowed volume required

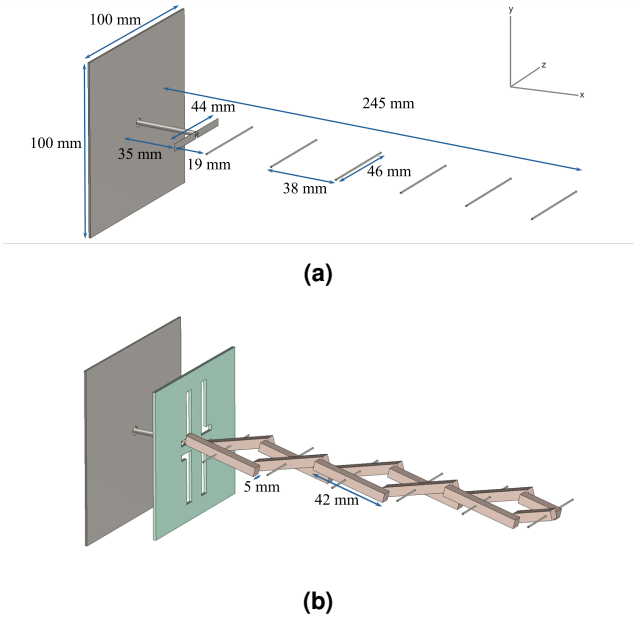


Figure 1: (a) CAD model of Yagi-Uda with dimensions. (b) Pantograph structure and antenna with structural dimensions.

during launch. Many types of deployable antennas have been utilised on CubeSats, spanning a range of frequencies, directivities, and applications. Antennas such as whips are often used for relatively low frequency telemetry, tracking, and command (TT&C), owing to their low-gain and reliable electromagnetic and mechanical performance [10]. These antennas utilise a simple sprung deployment, in which the coiled antenna unwinds once a release mechanism is triggered. Helical antennas are widely used in satellite applications and offer high-gain performance at similar frequencies (UHF) in a compact stowed volume, alongside innate circular polarisation [11]. They typically deploy using elastic potential energy stored within the helical structure, with one design achieving a stowed volume of 5% of the deployed volume [12]. Conversely, for very high-gain performance at higher frequencies, deployable parabolic reflector antennas can be used, such as in [7]. However, the deployment mechanism is complex, good alignment of the feed and reflector is required, and the reflector size becomes large when operating at relatively lower frequencies.

This publication presents a high-gain 8-element Yagi-Uda which operates across the 2.4 GHz ISM frequency band and fits onto the 10×10 cm face of a 3U CubeSat for IoT communication and sensing purposes. The work focusses on the antenna implementation rather than the mechanical design, and the proposed design serves as a breadboard model, in which the antenna has been optimised while the pantograph deployment actuation has not yet been implemented. An earlier version of this work was presented at the 2026 20^{th} European Conference on Antennas and Propagation (EuCAP) [13]. This is an extension of the work, demonstrating a refined pantograph design, improved antenna performance, the consideration of the CubeSat chassis on the antenna performance, and further antenna measurements for partial- and failed-deployments. This paper is organised as follows: Section 2 discusses the antenna and mechanical design, explaining how the deployment mechanism functions. Section 3 presents the simulated and measured results of the deployed antenna, with Section 4 further evaluating the antenna performance. The paper is concluded in Section 5, and possible future work on the design is proposed in Section 6.

2. Antenna Structure and Design

2.1. Yagi-Uda Design

The 8-element Yagi-Uda follows conventional design principles [14]. Fig. 1(a) details the dimensions of the elements, where the reflector plane is the 1U face of a 3U CubeSat, and the six director elements are 0.38λ long. The driven element is a planar dipole on 1.5 mm thickness FR4 ($\varepsilon_r \approx 4.3$), and has a length of 0.36λ—slightly shorter than a conventional half-wave dipole to account for the effective permittivity of the dielectric. The spacing between the reflector and the driven element is 0.29λ. The spacing between director elements is 0.31λ, and the spacing between the driven element and first director is half of this: 0.16λ. This is due to geometrical constraints of the pantograph structure, and was found to have little effect on the antenna performance. The director elements are brass rods of 1 mm diameter, and a length of flexible coaxial cable is used to feed the dipole through the reflector plane.

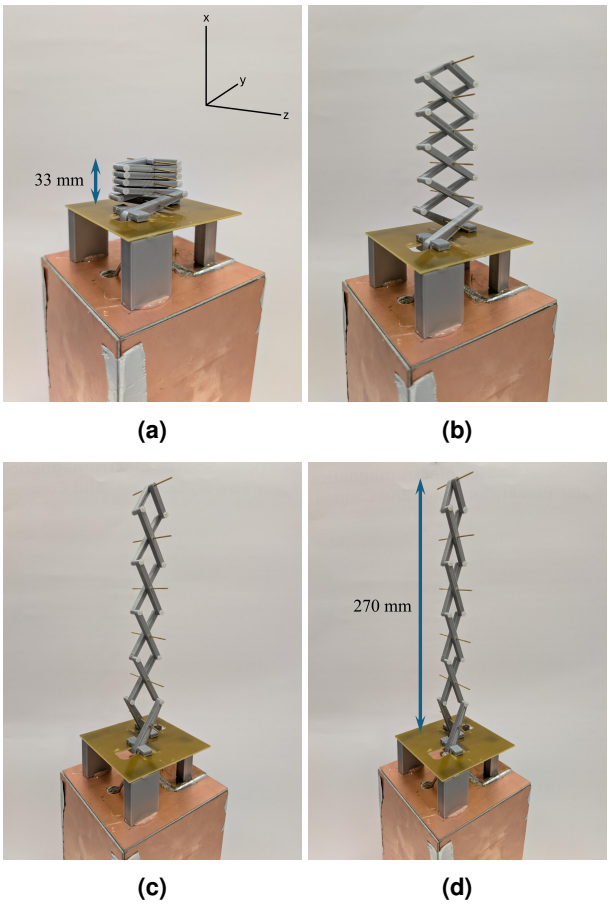


Figure 2: Deployment stages of pantograph structure: (a) stowed; (b) and (c) partially deployed; and (d) fully deployed.

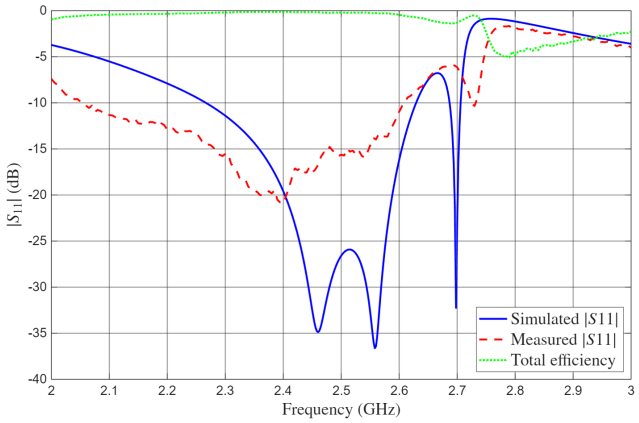


Figure 3: $|S_{11}|$ of simulated and measured antennas, and total efficiency of the measured antenna.

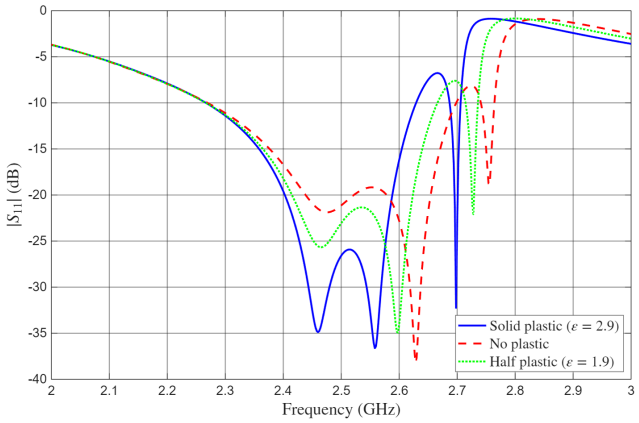


Figure 4: $|S_{11}|$ where the pantograph structure is simulated with varying effective permittivity.

2.2. Pantograph Structure

A pantograph structure is used for the deployment of the director elements, and acts as the boom of the Yagi-Uda once fully extended. A Yagi-Uda type antenna lends itself to this deployment mechanism due to the ability for the directors to be integral to the structure (acting as points of rotation during the extension), and since no electrical connection is needed between the elements. The movement of the pantograph is similar to that of a scissor lift, where each pair of 'arms' pivot around the respective director when the first two arms are separated or brought together. This movement either separates (flattening the structure) or brings together the arms (extending the structure) respectively. The movement and position of these arms are constrained with the cutouts on the dipole dielectric which act as a rail system for the first two arms to move along, ensuring the directors are in line with the driven element. The components used for the structure were fabricated of polylactic acid (PLA) using fused deposition modelling (FDM) technology on an Ultimaker 2+ 3D printer. An infill percentage of 20% was used—the plastic density was found to have little effect on the antenna performance in simulation.

Fig. 2(a) details the stowed dimensions, where the stowed length is 33 mm, and the total stowed volume is 29.7 cm^3. Fig. 2(d) shows the total deployed length of the pantograph as measured from the FR4 dielectric, which is 220 mm. Thus, a deployed-to-stowed length ratio of 6.7 is achieved. In this prototype, the deployment mechanism is considered primarily, focussing on the stow-ability and validity of using a pantograph, rather than the actuation method. Possible actuators are discussed in Section 6.

3. Results

3.1. Simulated Performance

The antenna was first modelled and validated in CST Studio without any structural components. These were subsequently added, and the model shown in Fig. 1(b) was optimised for 2.45 GHz. The solid blue line in Fig. 3 shows the simulated reflection coefficient. Taking −10 dB as a reference, the antenna operates between 2.27–2.63 GHz, with a bandwidth of 360 MHz (14.7% fractional bandwidth). The multiple resonances present at 2.46, 2.56, and 2.7 GHz are found to be due to the cutouts in the FR4 made for the pantograph structure.

Table 1: Antenna measurements taken at 2.45 GHz.

Parameter	Simulated	Measured
-10 dB bandwidth	360 MHz	560 MHz
Fractional bandwidth	14.7%	22.9%
Gain	11.8 dBi	11.9 dBi
SLL (E-plane)	−9.1 dB	−9.3 dB
SLL (H-plane)	−13.2 dB	−15 dB
HPBW (E-plane)	52.3°	52.3°
HPBW (H-plane)	47.3°	42.0°
Co-pol directivity	11.8 dBi	11.8 dBi
Cross-pol directivity	−1.6 dBi	−2.3 dBi
Radiation efficiency	99%	99%

Fig. 6(a) depicts the total far-field radiation pattern of the Yagi-Uda, and Fig. 8(a) and (b) show the principal plane cuts. The gain at boresight is 11.8 dBi. The half power beamwidths (HPBW) are 52.3° and 47.3° for the E- and H-plane respectively. Table 1 lists the full results of the simulated antenna.

The design was optimised with the pantograph structure modelled as solid plastic with $\varepsilon_r = 2.9$ [15]. The effect of these components was investigated by running simulations without the pantograph. As is often done when 3D printing, a partial infill was used which resulted in a lower effective permittivity. Fig. 4 shows the simulated results with no plastic structure, a partially filled plastic structure, and a solid plastic structure. The permittivity of the partially filled plastic is taken as $\varepsilon = 1.9$, representing approximately 50% air by volume [16]. Including the 3U CubeSat platform in the simulation increased the gain by 0.1 dBi due to the larger total aperture of the structure.

3.2. Measured Performance

The measured and simulated results agree well. The radiation pattern measurements were taken with the antenna mounted on a 3U CubeSat model, shown in Fig. 5. Fig. 3 shows the measured $|S_{11}|$ of the Yagi-Uda in a red dashed line, and Table 1

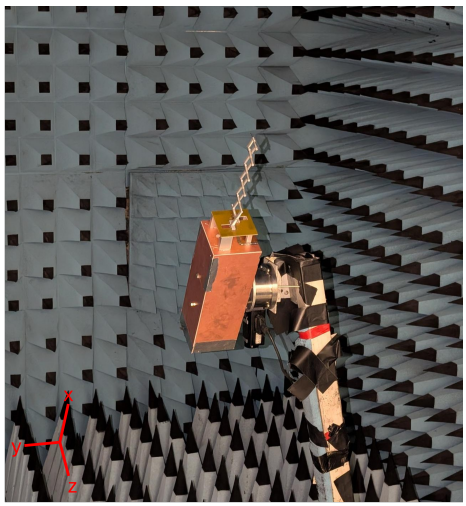


Figure 5: Antenna mounted on a 3U CubeSat chassis as measured in the anechoic chamber.

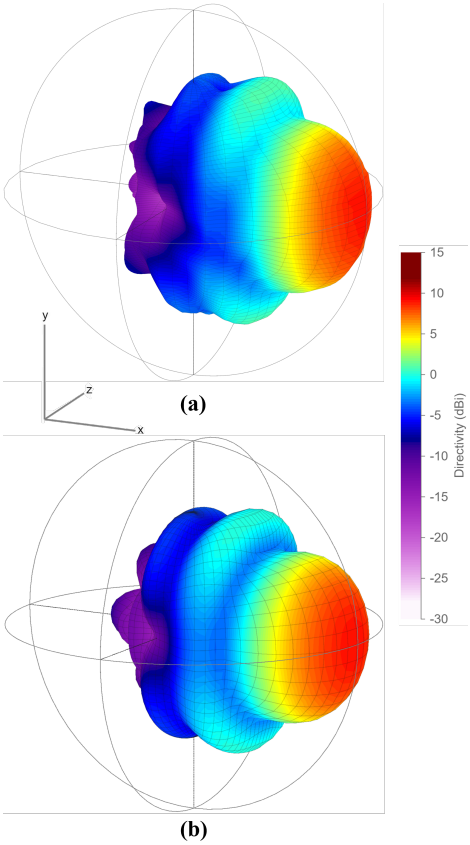


Figure 6: (a) Simulated and (b) measured radiation patterns.

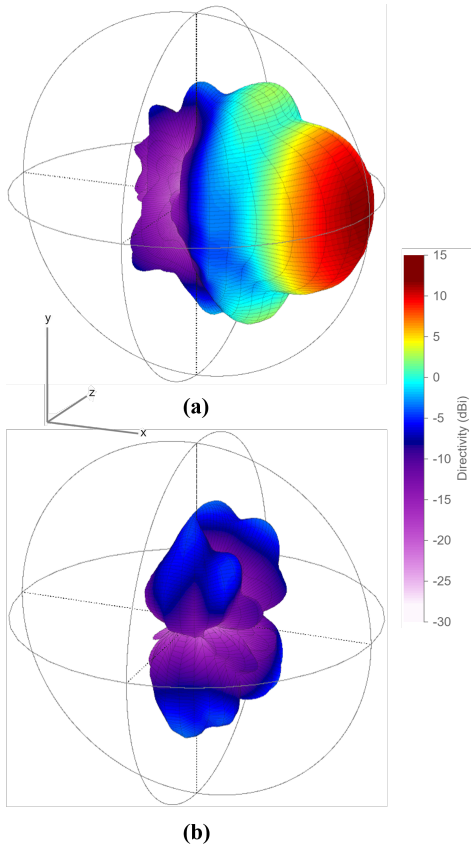


Figure 7: (a) Co- and (b) cross- polarisation measured 3D radiation.

presents the key results. The bandwidth covers the entirety of the 2.4 GHz ISM band, thus meaning the antenna can be used for IoT communication/sensing purposes in this frequency range. The -10 dB bandwidth is 560 MHz, and the $|S_{11}|$ minimum is negatively shifted when compared to the simulated results. The total efficiency of the antenna is 96% at 2.45 GHz, and is denoted by the dotted green line in Fig. 3. This value is calculated with $(1-|S_{11}|^2) \times \eta_{rad}$.

The total 3D far-field radiation pattern shown in Fig. 6(b) also aligns well with the simulated result. Fig. 8(a) and (b) show the principal plane cuts for co- and cross-polarisation, and total radiated power. It is worth noting that much of the cross-polarisation contribution cannot be seen in these plane cuts when compared to the 3D cross-polarisation pattern, shown in Fig. 7(b). The gain is 11.9 dBi, with a radiation efficiency of 99%. This was calculated by comparing the total radiated power to a reference antenna, in this case a monopole [17]. Fig. 7(a) and (b) shows the co- and cross-polarisation radiation patterns respectively, where it can be seen that the antenna has high linear polarisation purity.

Both simulated and measured radiation patterns have two main side lobes, evident in the E-plane, which are approximately in the y and y-x direction. It can be inferred from the polarisation plots that these side lobes are primarily caused by the cross- and co-polarisation far-fields respectively. There are nulls present in both polarisations along the z-axis, which is characteristic of a dipole antenna.

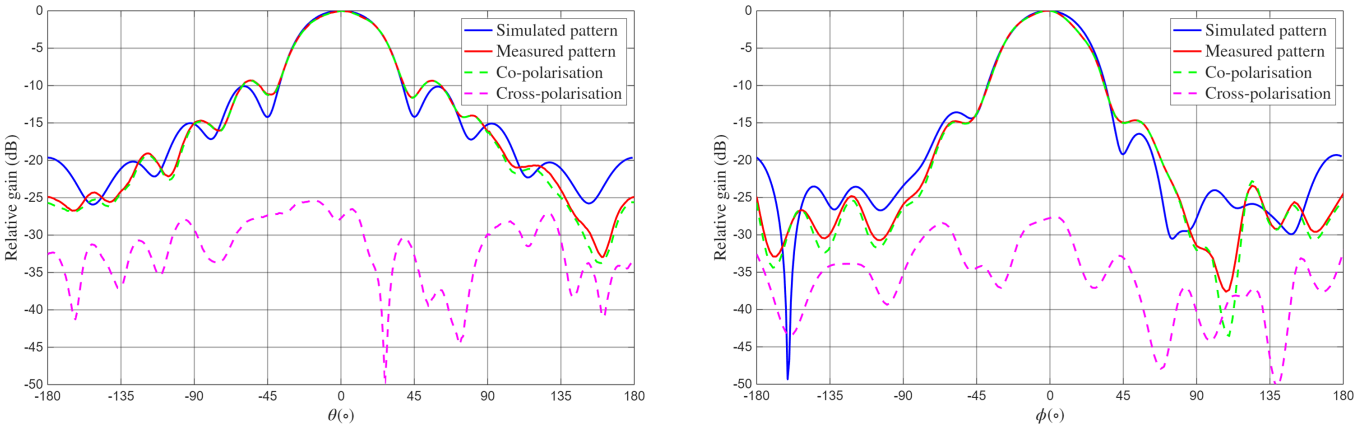


Figure 8: Cartesian cuts in the (a) $\phi = 0^\circ$ plane, and (b) $\theta = 90^\circ$ plane.

4. Further Measurements and Designs

If the antenna fails to deploy successfully, the mission can be a partial or total failure. The ViaSat-3 satellite launched in 2023 experienced a failure in the deployment of the main reflector antenna, leading to a performance reduction of 90% [18]. Thus, the Yagi-Uda was also measured at two stages of failure: total and partial (half-deployed).

Table 2 lists the results for the two failure cases of the antenna considered, with the measured values aligning well with equivalent simulations of the antenna. Fig. 2(a) shows the antenna in a stowed state (i.e., total deployment failure, and (b) shows the antenna in a partially deployed state (pantograph length approx. 110 mm). The measured reflection coefficients are shown in Fig. 9, where the partial deployment has a deep resonance at the operational frequency of 2.45 GHz, indicating the antenna would still be usable. In the case of a total deployment failure, the main resonance shifts to 2.6 GHz, with an $|S_{11}|$ of -13.4 dB at 2.45 GHz.

Fig. 10 depicts the far-field radiation patterns for (a) partial and (b) total deployment failure of the antenna. In comparison to the fully deployed measured far-field, the partial deployment has higher side-lobe levels and a decreased maximum gain of 11.1 dBi. In the case of a total deployment failure, the beamwidth is widened significantly, with the main beam and side lobes merging into a single beam, and a gain of 9.3 dBi. Furthermore, the radiation efficiency is decreased for both. In either case of deployment failure, the system would still be operational, albeit with slightly reduced performance.

A common method to increase the directivity of a Yagi-Uda type antenna is to increase the total number of director elements. Previous work investigated a deployable Yagi-Uda with three directors [13], with this paper extending the antenna to six directors. It was found that increasing the number of directors past six yielded diminishing gains in directivity for the corresponding increase in volume. Each additional element requires two more pantograph components, and so a trade-off must be made of enhanced directivity against stowed volume.

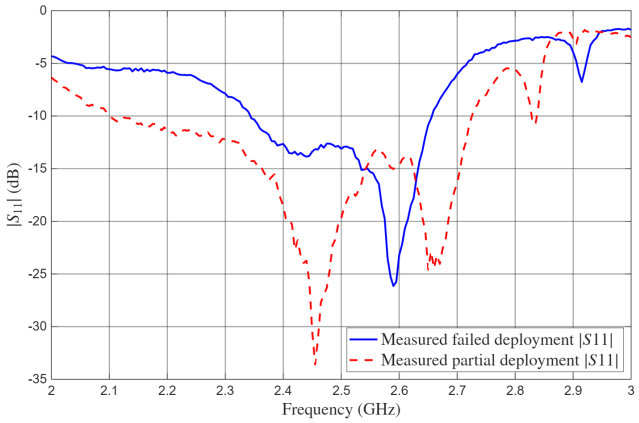


Figure 9: Measured $|S_{11}|$ of partial and failed deployment of antenna.

5. Conclusion

The design and measured results of a deployable Yagi-Uda antenna operating in the 2.4 GHz ISM band which fits on the end-face of a 3U CubeSat has been presented. A high-gain of 11.9 dBi has been achieved at the operational frequency of 2.45 GHz, and a pantograph-based deployment system for the antenna boom has been described and tested. A deployed-to-stowed length ratio of 6.7 has been achieved, with a stowed volume of 29.7 cm^3, a stowed length of 33 mm, and a deployed length of 220 mm. The antenna performance has been investigated in the event of a deployment failure, and it has been shown that the antenna would still be operational in this situation, albeit with reduced performance. The measured results align with the simulation across the desired band, and prove the validity of the proposed design. Thus, there is scope for the mechanism to be used for other frequencies, such as the lower IoT band of 868/915 MHz.

6. Future Work

The antenna design can be developed further in regards to both the electromagnetic and mechanical performance. Exploring

Table 2: Partial and full deployment failure results at 2.45 GHz.

Parameter	Partial Failure	Total Failure
$\|S_{11}\|$	−13.4 dB	−30.4 dB
Gain	11.1 dBi	9.3 dBi
Co-pol directivity	11.0 dBi	9.2 dBi
Cross-pol directivity	−1.9 dBi	−4.4 dBi
Radiation efficiency	93%	89%

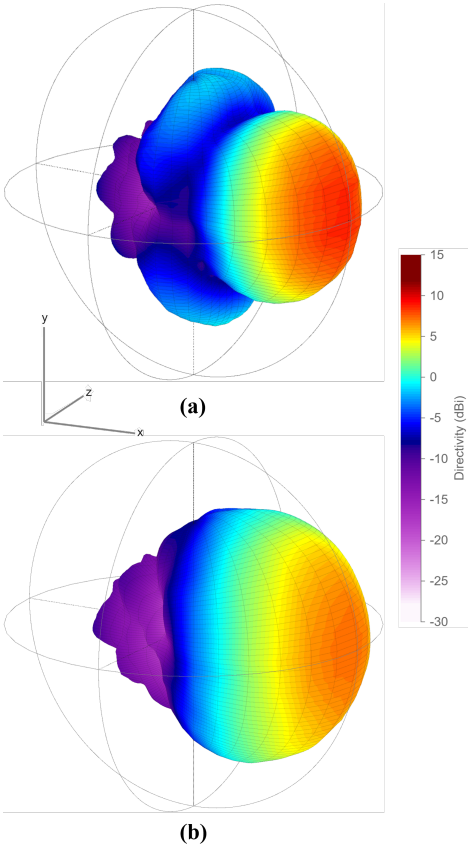


Figure 10: (a) Partial deployment failure and (b) total deployment failure radiation patterns.

the possibility of implementing crossed elements would permit dual linear or circular polarisation. Dual polarisation would allow two concurrent data streams, whereas circular polarisation would reduce the likelihood of polarisation misalignment between the satellite and ground station antenna. As mentioned prior, redesigning the antenna such that the operational frequency covers the 868/915 MHz would allow IoT devices, such as those which are LoRa-enabled, in this band to be communicated with or sensed. The length of the elements may be too large to fit on the small face of the CubeSat, and so a loop Yagi-Uda utilising a similar deployment mechanism may be more suitable.

There is also scope for further work on the mechanical structure of the antenna. Integrating an actuator for the pantograph boom is perhaps the most pertinent, to pull the base of the pantograph arms together, extending the boom. There are various options for this, such as a screw-drive, miniature motor system, shape memory alloy, or a spring system. The impact of these on the antenna performance must be investigated, however. Similarly, a second deployment must be used to create the separation between the reflector plane (i.e., the CubeSat face), and the driven element. Additionally, the materials used in this model are not space-grade, and also provide general scope for improvement. A higher quality and space-rated dielectric, such as Rogers 5880, should be utilised instead of the FR4 substrate used in this model. Similarly, a higher quality plastic should be used for the pantograph boom. For example, polyether ether ketone (PEEK) is more suited to this application, but suffers from high cost and is difficult to work with.

Mechanical testing should also be considered to ensure the pantograph structure could withstand both the launch and operational periods without suffering from physical failures and degradation. These tests may include: acceleration, vibration (random and sinusoidal), and thermal cycling tests [19].

References

[1] M. N. Sweeting, "Modern small satellites-changing the economics of space," *Proceedings of the IEEE*, vol. 106, no. 3, pp. 343–361, Mar. 2018.

[2] ESA, "Report on the Space Economy 2024," The European Space Agency, Tech. Rep., Oct. 2024. [Online]. Available: https://space-economy.esa.int/documents/b61btvmeaf6Tz2osXPu712bL0dwO3uqdOrFAwNTQ.pdf

[3] "Space systems—cube satellites (CubeSats)," International Organization for Standardization, Geneva, Standard ISO 17770:2017, Jun. 2017.

[4] E. Kulu, "CubeSats & Nanosatellites - 2024 statistics, forecast and reliability," in *31st IAA Symposium on Small Satellite Missions*. Milan, Italy: International Astronautical Federation (IAF), 2024, pp. 601–614.

[5] C. Cappelletti and D. Robson, "CubeSat missions and applications," in *Cubesat Handbook*. Elsevier, 2021, pp. 53–65.

[6] N. Chahat, E. Thiel, J. Sauder, M. Arya, and T. Cwik, "Deployable one-meter reflectarray for 6U-class CubeSats," in *2019 13th European Conference on Antennas and Propagation (EuCAP)*, Mar. 2019, pp. 1–4.

[7] N. Chahat, J. Sauder, R. Hodges, M. Thomson, Y. R. Samii, and E. Peral, "Ka-band high-gain mesh deployable reflector antenna enabling the first radar in a CubeSat: RainCube," in *2016 10th European Conference on Antennas and Propagation (EuCAP)*, Apr. 2016, pp. 1–4.

[8] J. Costantine, Y. Tawk, C. G. Christodoulou, J. Banik, and S. Lane, "CubeSat deployable antenna using bistable composite tape-springs," *IEEE Antennas and Wireless Propagation Letters*, vol. 11, pp. 285–288, 2012.

[9] A. C. M. Austin, T. Pelham, G. Hilton, and M. A. Beach, "Robust deployable reflectors for antennas on Cubesats," in *42nd ESA Antenna Workshop*, Nov. 2024.

[10] S. Abulgasem, F. Tubbal, R. Raad, P. I. Theoharis, S. Lu, and S. Iranmanesh, "Antenna designs for CubeSats: A review," *IEEE Access*, vol. 9, pp. 45 289–45 324, 2021.

[11] J. D. Kraus, *Antennas*, 2nd ed. New York: McGraw-Hill, 1988.

[12] L. Alminde, K. Kaas, M. Bisgaard, J. Christiansen, and D. Gerhardt, "GOMX-1 flight experience and air traffic monitoring results," *Small Satellite Conference*, Aug. 2014.

[13] C. M. Lambe, G. S. Hilton, and A. C. M. Austin, "Deployable L-Band Yagi-Uda antenna for a 3U cubesat using a pantograph mechanism," in *2026 20th European Conference on Antennas and Propagation (EuCAP)*, 2026, pp. 1–4.

[14] Y. Huang and K. Boyle, *Antennas: from Theory to Practice*. Chichester, UK: John Wiley & Sons, 2008.

[15] C. Dichtl, P. Sippel, and S. Krohns, "Dielectric properties of 3D printed polylactic acid," *Advances in Materials Science and Engineering*, vol. 2017, no. 1, pp. 1–10, Jul. 2017.

[16] J. Persad and S. Rocke, "Impact of 3D printing infill patterns on the effective permittivity of 3D printed substrates," *IEEE Journal of Microwaves*, vol. 4, no. 2, pp. 277–292, Apr. 2024.

[17] H. Giddens, D. Paul, G. Hilton, and J. McGeehan, "Numerical and experimental evaluation of phantoms for off-body wireless communications," in *2011 Loughborough Antennas & Propagation Conference*, Nov. 2011, pp. 1–4.

[18] J. Rainbow, "ViaSat-3 failure investigation to conclude next week," Nov. 2023. [Online]. Available: https://spacenews.com/viasat-3-failure-investigation-to-conclude-next-week/

[19] European Cooperation for Space Standardization Secretariat, "Space Engineering Testing," Standard ECSS-E-ST-10-03C Rev.1, May 2022.